Final Draft
of the original manuscript:

Martins, R.M.S.; Schell, N.; Mahesh, K.K.; Pereira, L.; Silva, R.J.C.;
Braz Fernandes, F.M.:

Texture Development and Phase Transformation Behavior of Sputtered Ni-Ti Films

In: Journal of Materials Engineering and Performance (2009) ASM International

DOI: 10.1007/s11665-009-9484-9

Texture development and phase transformation behavior of sputtered Ni-Ti films

R.M.S. Martins[1,2,*], N. Schell[3], K.K. Mahesh[2], L. Pereira[2], R.J.C. Silva[2], F.M. Braz Fernandes[2]

[1]Institute of Ion Beam Physics and Materials Research, Forschungszentrum Dresden-Rossendorf, P.O. Box 510119, 01314 Dresden, Germany

[2]CENIMAT/I3N, Campus da FCT/UNL, 2829-516 Monte de Caparica, Portugal

[3]GKSS Research Center Geesthacht, Max-Planck-Str. 1, 21502 Geesthacht, Germany

ABSTRACT

It is essential to identify and control the preferential orientation of Ni-Ti Shape Memory Alloy (SMA) films since it is a crucial factor in determining the shape memory behavior. In the present work *in-situ* studies by synchrotron radiation scattering enabled to identify the different steps of the structural evolution of Ni-Ti films during co-sputtering deposition.

For micro-electromechanical systems (MEMS) integration, there is a need for an electrically and thermally insulating or sacrificial layer. Widening the scope of previous experiments concerning the influence of the deposition parameters on the structure of the Ni-Ti films, the incorporation of a TiN buffer layer has been tested. Here, it is established a relationship between the TiN substrates and Ni-Ti texture development (B2 phase).

Ni-Ti films mainly containing grains with (110) or (211) planes of the B2 phase parallel to the film surface could be produced using TiN buffer layers with distinct thickness values. The electrical resistivity measurements performed during temperature cycling have shown that the crystallographic orientations of the Ni-Ti films influence their phase transformation characteristics. The resistivity increase during R-phase transformation, especially visible on cooling, is higher for Ni-Ti films with a higher fraction of grains of the B2 phase with (211) parallel to the film surface.

* E-mail: rmsm@fct.unl.pt; Fax: +351.21.294.85.58

Keywords:

deposition by sputtering; *in-situ* x-ray diffraction; Ni-Ti; Shape Memory Alloy; phase transformation behavior; texture development.

1. Introduction

In physical vapour deposition (PVD) processes the atoms are deposited from a gas phase onto a substrate and the deposition parameters play an important role in determining the microstructure and physical properties of the grown films [1]. There are some published structure-zone models in the literature to describe the observed morphology of PVD grown films [2]. However, Hultman and Sundgren [3] referred that though the structure zone models seem to be adequate in giving a qualitative classification of film microstructure formation, they do not include effects from the substrate material itself on the film growth mode. It has been found that the observed microstructure of hard coatings is not simply dependent on process parameters such as temperature and energetic particle bombardment during growth, but also significantly dependent on the substrate crystal structure, morphology, composition and/or surface contamination, all of which have important influences on the nucleation. For example, substrate surface roughness often exists at the same time on several size scales. This roughness can be reproduced in exaggerated form on the coating surfaces in *zone I* structures, due to superimposed shadow growth. It is also essential to choose the substrate material carefully since preferred crystallographic orientation in coatings have been associated with effects such as minimization in surface energies and a variation in condensation coefficients [4].

The composition and structure of sputtered Ni-Ti Shape Memory Alloy (SMA) films are significantly affected by the sputtering conditions: target power, gas pressure, target to substrate distance, deposition temperature, substrate bias voltage *etc* [5-10]. Additionally, important issues like formation of film texture and its control are not yet understood. It is fundamental to identify and control their preferential orientation, as it is a crucial factor in determining the extent of the strain recovery [11]. For micro-electro-mechanical systems (MEMS) integration, there is a need for an electrically and thermally insulating or sacrificial layer [12,13]. Therefore, the study of Ni-Ti film deposition on different types of substrates is an important topic of research.

In the present work, naturally oxidized Si(100) wafers as well as TiN buffer layers have been used as substrates for Ni-Ti deposition. Crystallized near equiatomic Ni-Ti films have been obtained at the end of the deposition, exhibiting distinct crystallographic orientations depending of the substrate type. It has been established a relationship between the substrates and texture development.

In order to achieve the goals proposed for this work, a two-magnetron sputter deposition chamber has been used allowing to heat and to apply a bias voltage to the substrate. This equipment could be mounted into the six-circle diffractometer of the Rossendorf Beamline (ROBL) [14] at the European Synchrotron Radiation Facility (ESRF), enabling an *in-situ* characterization by x-ray diffraction (XRD) of the films during their growth. In addition to the *in-situ* studies, complementary *ex-situ* characterization techniques such as electrical resistivity (ER) measurements during temperature cycling have been used to characterize the transformations characteristics of the Ni-Ti samples. Wang *et al.* [15], based in a previous work [16] reported that the greater the extent of sub micro twinning, the higher the increase in the resistivity. They also mentioned the finding of Cross *et al.* [17], i.e., there is a one-to-one correspondence between the mechanical "memory" effect and the ER curve; the larger the electrical resistivity "peak" [between austenite start temperature (A_s) and martensite finish temperature (M_s)] the more pronounced is the "memory" effect (i.e., the shape recovery performance).

2. Experimental details

The sputtering experiments were carried out in the D.C. magnetron sputtering chamber that has been described elsewhere [18]. Two unbalanced magnetrons, equipped with a 25.4 mm Ni-Ti target (49 at% Ni – 51 at% Ti) and a 25.4 mm Ti target (purity 99.99%), respectively, were positioned at a distance of 100 mm from the substrate. They are each tilted 30° away from the substrate normal, including their cylindrical chimneys. Figure 1 shows the actual mounting of the deposition chamber in the Huber goniometer at ROBL.

Pieces of size 15×15 mm^2, cut from naturally oxidized Si(100) wafers (oxide layer of ≈ 2 nm) and thermally oxidized Si(100) wafers (with a 140 nm amorphous SiO_2 capping layer), have been used as substrates. The base pressure at the deposition temperature of ≈ 470°C was 2×10^{-5} Pa and the working pressure during deposition was 0.42 Pa. For the deposition of the TiN buffer layers, the Ti target was run at a constant power of 80 W with an Ar/N_2 gas flow of 2/0.5 sccm and for the Ni-Ti films the Ni-Ti and Ti magnetrons were driven at a power of 40 and 20 W, respectively. The Ni-Ti films exhibited final compositions values of approximately

50 at.%Ni–50 at.%Ti (compositional results obtained from the combination of Rutherford backscattering spectroscopy and Auger electron spectroscopy techniques – results not shown here). Selected processing conditions of the samples studied are presented in Tab. 1.

The x-rays were monochromatized to 18.367 keV (0.0675 nm) for the in-situ studies at ROBL. Two different scattering geometries were employed: (1) off-plane (vertical) large-angle XRD in Bragg-Brentano geometry. This method provides a measure for the off-plane texture when comparing the peak areas. (2) Low-angle specular x-ray reflectivity (XRR) has been performed for the study of the thinner TiN layers. Information on film density and surface roughness has been obtained, and from the Kiessig fringes the film thickness has been determined. This was achieved using the Bede REFS computer code to fit the data [19].

In order to investigate the phase transformations, the temperature dependence of the ER of the samples was measured using the four-probe van der Pauw geometry (BIO-RAD HL 5550). The thermal cycles comprised (i) heating from room temperature (RT) up to 110ºC, followed by (ii) cooling down to −110ºC, and finishing by (iii) heating up to 110ºC. The analysis of the transformation characteristics was based on the cycles (ii) and (iii). The measurements were performed with the Ni-Ti films attached to the substrate.

3. Results and Discussion

Experimentally, the growth of four Ni-Ti samples was studied. The varying deposition parameter was the substrate type, i.e., Ni-Ti films were deposited directly on naturally oxidized Si(100) and on TiN grown on thermally oxidized Si(100) substrates (Tab. 1). TiN buffer layers of thickness of approximately 15, 80 and 215 nm were chosen (corresponding to 3, 15 and 40 min deposition, respectively).

Figure 2 shows the variation of the net areas of the diffraction peaks of the Ni-Ti B2 phase as a function of deposition time (peaks observed during growth):

(i) B2(110) and B2(200) peaks for the Ni-Ti film deposited directly on naturally oxidized Si(100) substrate;

(ii) B2(110) and B2(211) peaks for the Ni-Ti film deposited on a TiN buffer layer with a thickness of ≈ 15 nm;

(iii) B2(110) peak for the Ni-Ti film deposited on a TiN buffer layer with a thickness of ≈ 215 nm.

In the case of the film deposited directly on the naturally oxidized substrate, after the growth of an initial layer with the {200} planes parallel to the surface during the first 30 min (≈ 180 nm thick, taking into account that the growth rate was estimated as ≈ 0.1 nm/s), the B2(200) peak intensity saturated and stayed constant. The B2(110) peak intensity was linearly growing, starting from the B2(200) peak intensity stabilization, until the end of the deposition. The experiments on the growth of Ni-Ti on TiN buffer layers have shown that the B2(200) diffraction peak is hardly detected (in contrast to the depositions on oxidized Si substrates) and, thus, not considered for this representation.

A key role is attributed to the amorphous Si oxide layer on the initial preferential stacking of the B2 phase with (*h*00) planes parallel to the film surface during the initial growth stage. This has been demonstrated by the use of thermally oxidized Si(100) substrates [20]. Kim *et al.* [21] proposed that a strong interfacial adsorption on the heated substrate promotes the preferential coverage by a first layer of Ti on top of thermally oxidized Si substrates. This leads to the preferential formation of the (*h*00) oriented Ni-Ti film since, in the B2 cubic structure, the (*h*00) planes are alternately occupied by Ti and Ni atoms. For depositions of Ni-Ti on TiN buffer layers there is no Ni-Ti/SiO_2 interface and, therefore, the development of the (100) orientation of B2 phase parallel to the substrate surface is not observed.

TiN films grown by vapour phase deposition techniques usually have a preferred growth orientation that varies according to the growth conditions. The orientations most often observed are <100> and <111> (<hkl> grains are here defined as grains with a plane from the {hkl} family parallel to the film surface). Primarily <100> and <111> oriented grains nucleate during the initial stages of growth but, with increasing film thickness, the development of a preferred layer orientation either <100> or <111> is observed. The deposition parameters selected for the growth of the TiN buffer layers used in the present study led to the nucleation and growth of <100> and <111> oriented grains during the initial stages of film growth and <111> grains taking over at larger thickness values. TiN(111) and TiN(200) diffraction peaks could be

observed for thickness values of approximately 80 and 215 nm (no peaks could be detected for the thinner TiN layer of ≈ 15 nm). However, only for a TiN layer with ≈ 215 nm it is possible to conclude that <111> grains dominate (results presented in Ref. [22]).

Figure 2 shows that in the case of the deposition of Ni-Ti on the TiN film with a thickness of ≈ 15 nm, the 110 diffraction peak of the B2 phase of Ni-Ti (in Bragg–Brentano geometry) dominated at the beginning of the deposition, while the B2(211) diffraction peak assumed higher values at a later stage of the deposition. It suggested that for this thinner TiN layer (≈ 15 nm) a rough or granular surface with different crystal facets plays an important role on the growth direction of the columnar crystals of Ni-Ti, together with the fact that the targets are tilted 30° away from the substrate normal. During the initial Ni-Ti deposition period, there is a (110) stacking and a columnar growth such that <110> lies close to the substrate normal. This type of stacking is due to the fact that (110) is the more densely packed crystallographic plane for the B2 structure [23]. However, due to the surface morphology of the TiN layer (without a dominating crystallographic orientation – most likely a granular uneven surface) and the geometrical shadowing effects, as growth proceeds the growth direction is more influenced by the direction of incident particles. Columnar grains stacking on (110) will then grow tilted to the surface normal (towards the magnetron with the Ni-Ti target running at 40 W) due to the shadowing effects. This tilting leads to (211) planes more closely parallel to the substrate surface and a higher intensity of the corresponding diffraction peak. Thus, it is suggested that this crystallographic orientation development (for the Ni-Ti sample with a TiN buffer layer with a thickness of ≈ 15 nm) is associated to the combined effects of low surface mobility and shadowing. Although the results are not shown in Fig. 2 this behaviour could be expected for the deposition of Ni-Ti on a TiN buffer layer with a thickness of ≈ 80 nm. It has been mentioned above that in both cases a dominating orientation could not be identified for the TiN buffer layers (of roughly 15 and 80 nm), i.e., <100> and <111> oriented grains of TiN nucleated and grew. In contrast, the deposition of Ni-Ti on TiN with a topmost layer formed mainly by <111> oriented grains showed a preferential growth of <110> oriented grains of the Ni-Ti B2 phase from the beginning of the deposition, with a constant growth rate during the whole deposition.

A typical XRR result obtained *in situ* for a TiN layer after 3 min deposition is shown in Fig. 3. This technique allowed to calculate the growth rate for the TiN buffer layers (≈ 0.086 nm/s) since the thickness is obtained from the fitting procedure. The TiN layer exhibits a density of ≈ 97 % (≈ 5.27 g/cm^3) of the bulk density (5.43 g/cm^3). From the fitting an average roughness of ≈ 0.9 nm was derived. However, although XRR provides valuable information it is in general useful only for lower film thicknesses. TiN buffer layers with thickness values larger than ≈ 100 nm could hardly be resolved by the reflectivity experiments because of interference with the SiO_2 buffer layer. Therefore, XRR technique did not allow a direct comparison of the roughness values of the thinner TiN buffers layers with the thicker layer (with ≈ 215 nm). Nevertheless, it is believed that the distinct surface morphology of the TiN layers with different thickness values has an important role on the adatoms surface mobility and shadowing effects. Most likely, the TiN film roughness is related with texture and film roughness is determined by crystal habit. The ROBL team has been working on TiN for several years [24] and these comments are also based in previous observations.

XRD obtained at RT and 470°C (after deposition) by means of synchrotron radiation at ROBL for the Ni-Ti samples with TiN are shown in Fig. 4. The experimental set-up used at ROBL for the study of the Ni-Ti samples with TiN buffer layers of approximately 80 and 215 nm did not allow the study of the B2(211) peak angular range at 470°C. Thus, the samples have also been studied ex-situ (without angular range restrictions) at a laboratory source (diffractometer D-5005 from BRUKER AXS) at 100°C (austenitic state) in order to record the B2(211) diffraction peak. The respective results are shown in the inset (top). These results show similar B2(211) peak shape and peak intensity for the Ni-Ti films deposited on TiN with total thickness values of roughly 15 and 80 nm. At RT the Ni-Ti film structure was mainly rhombohedral (R-phase) as shown by the bottom diffractograms of Fig. 4. With the increase of temperature to 470°C it transformed to B2 phase (top diffractograms). During the transformation from the high temperature phase (B2) to the rhombohedral R-phase while cooling, the height of the B2(110) diffraction peak decreased, splitting into two resolvable R(112) and R(300) peaks. This was especially visible in the case of the Ni-Ti film deposited on top of a TiN layer with a thickness of ≈ 215 nm. Furthermore, it was perceptible a splitting of the B2(211) peak into the (033) and (141) peaks of the R-phase structure for the samples with TiN layers of about 15 and 80 nm.

The temperature dependence results of the ER of the Ni-Ti samples with TiN buffer layers of thickness approximately 15, 80 and 215 nm are shown in Fig. 5 for cooling (top curves) and heating (bottom curves). In the figure, R_s, R_f, M_s, M_f are the temperatures for the start and finish of the formation of the *R*-phase and martensite (B19'), on cooling, and R'_s, R'_f, A_s, A_f are the temperatures for the start and finish of the formation of the *R*-phase and the B2 phase, on heating. For the different samples, as the temperature decreases, an increase in the resistivity values was observed (B2 $\Rightarrow$ R–phase transformation), followed by a decrease associated with the R–phase $\Rightarrow$ B19' transformation. During heating the transformation was also occurring in two steps, B19' $\Rightarrow$ R–phase $\Rightarrow$ B2 as observed by the respective increase in the ER. However, during heating the increase in the ER was smaller than the one observed on cooling. Moreover, the increase of the ER during R-phase formation (on cooling and heating) is lower for the Ni-Ti sample with a TiN buffer layer of $\approx$ 215 nm.

According to the ER results obtained during temperature cycling, presented in Fig. 5, the distinct crystallographic orientations of the Ni-Ti films influence their phase transformation characteristics. The resistivity increase during R-phase transformation, on cooling and heating, was higher for Ni-Ti films with a higher fraction of grains of the B2 phase with (211) parallel to the film surface. Therefore, the use of a TiN buffer layer is an important finding for the control of the crystallographic orientations of the Ni-Ti SMA films and consequently to influence their phase transformation characteristics.

4. Conclusion

The *in-situ* XRD measurements have shown that on naturally oxidized Si(100) substrates, without a substrate bias voltage, the Ni-Ti B2 phase starts by stacking onto (*h*00) planes (due to the native oxide layer), and as the thickness increases, evolves into a <110> preferential orientation. In the case of a Ni-Ti film deposited on TiN with a topmost layer formed mainly by <111> oriented grains, there is a preferential growth of <110> oriented grains of the Ni-Ti B2 phase from the beginning of the deposition, with a constant growth rate during the whole deposition. For the Ni-Ti films deposited on top of a TiN layer where a dominating orientation could not be identified (i.e., <100> and <111> oriented grains of TiN nucleated and grew), a different behaviour is observed, that is, <110> oriented grains of the Ni-Ti B2 phase dominate at lower thickness values, while the B2(211) planes parallel to the substrate surface take over at higher

thickness values (due to an inclination of (110) of the columnar grains relative to the substrate normal).

The ER results obtained during temperature cycling have shown that the distinct crystallographic orientations of the Ni-Ti films influence their phase transformation characteristics. The resistivity increase during R-phase transformation, noticeably on cooling, is higher for Ni-Ti films with a higher fraction of grains of the B2 phase with (211) parallel to the film surface.

ACKNOWLEDGMENTS

The authors thank the FCT/MCTES for a Ph.D. scholarship (POCI 2010/FSE for R.M.S.M.) and U. Strauch for his technical assistance during the measurements at ROBL. Financial support from the ESRF for the experiments at ROBL and from the FCT/MCTES for the pluriannual financial support of CENIMAT/I3N is gratefully acknowledged by K.K.M., L.P., R.J.C.S. and F.M.B.F.

REFERENCES

[1] J.A. Thornton, Influence of apparatus geometry and deposition conditions on structure and topography of thick sputtered coatings, J. Vac. Sci. Tecnol., 11**,** 1974, p 666-670, in English.

[2] P.B. Barna, and M. Adamik, Fundamental structure forming phenomena of polycrystalline films and the structure zone models**,** Thin Solid Films, 317, 1998, p 27-33, in English.

[3] L. Hultman, and J.E. Sundgren, Structure/Property Relationships For Hard Coatings, Handbook of Hard Coatings: Deposition Technologies, Properties and Applications, R.F. Bunshah, Noyes Publications, 2001, p 108-180.

[4] C.V. Thompson, Structure Evolution During Processing of Polycrystalline Films, Annu. Rev. Mater. Sci., 30, 2000, p 159-190, in English.

[5] J.D. Busch, A.D. Johnson, C.H. Lee, and D.A. Stevenson, Shape-memory properties in Ni-Ti sputter-deposited film, J. Appl. Phys., 68, 1990, p 6224-6228, in English.

[6] K.R.C. Gisser, J.D. Busch, A.D. Johnson, and A.B. Ellis, Oriented nickel-titanium shape memory alloy films prepared by annealing during deposition, Appl. Phys. Lett., 61, 1992, p 1632-1634, in English.

[7] A.P. Jardine, H. Zhang, and L.D. Wasielesky, Investigation into the thin-film fabrication of intermetallic NiTi, Mat. Res. Soc. Symp. Proc., 187, 1990, p 181-186, in English.

[8] K.K. Ho, K.P. Mohanchandra, and G.P. Carman, Examination of the sputtering profile of NiTi under target heating conditions, Thin Solid Films, 413, 2002, p 1-7, in English.

[9] A. Ishida, and V. Martynov, Sputter-deposited Shape-Memory Alloy thin films: properties and applications, MRS Bull., 27, 2002, p 111-114, in English.

[10] M.J. Vestel, D.S. Grummon, R. Gronsky, and A.P. Pisano, Effect of temperature devitrification kinetics of NiTi films, Acta Mater., 51, 2003, p 5309-5318, in English.

[11] Y.C. Shu, and K. Bhattacharya, The influence of texture on the shape-memory effect in polycrystals, Acta Mater., 46, 1998, p 5457-5473, in English.

[12] J.A. Walker, K.J. Gabriel, and M. Mehregany, Thin-film processing of TiNi shape memory alloy, Sens. Actuators, A21-A23, 1990, p 243-246, in English.

[13] Y. Fu, H. Du, W. Huang, S. Zhang, and M. Hu, TiNi-based thin films in MEMS applications: a review, Sens. Actuators A, 112, 2004, p 395-408, in English.

[14] W. Matz, N. Schell, G. Bernhard, F. Prokert, T. Reich, J. Claußner, W. Oehme, R. Schlenk, S. Dienel, H. Funke, F. Eichhorn, M. Betzl, D. Pröhl, U. Strauch, G. Hüttig, H. Krug, W. Neumann, V. Brendler, P. Reichel, M.A. Denecke, and H. Nitsche, ROBL – a CRG Beamline for Radiochemistry and Materials Research at the ESRF, J. Synchroton Radiat., 6, 1999, p 1076-1085, in English.

[15] F.E. Wang, S.J. Pickart, and H.A. Alperin, Mechanism of the TiNi martensitic transformation and the crystal structures of TiNi-II and TiNi-III phases, J. Appl. Phys., 43, 1972, p 97-112, in English.

[16] F.E. Wang, B.F. DeSavage, W.J. Buehler, and W.R. Hosler, The irreversible critical range in the TiNi transition, J. App. Phys., 39, 1968, p 2166-2175, in English.

[17] W.B. Cross, A.H. Kariotis, and F.J. Stimler, Nitinol characterization study, NASA Report, CR-1433, 1969.

[18] W. Matz, N. Schell, W. Neumann, J. Bøttiger, and J. Chevallier, A two magnetron sputter deposition chamber for in situ observation of thin film growth by synchrotron radiation scattering, Rev. Sci. Instrum., 72, 2001, p 3344-3348, in English.

[19] http://www.bede.co.uk

[20] R.M.S. Martins, N. Schell, M. Beckers, K.K. Mahesh, R.J.C. Silva, and F.M.B. Fernandes, Growth of sputter-deposited Ni-Ti thin films: effect of a SiO_2 buffer layer, Appl. Phys. A: Mater. Sci. & Proc., 84, 2006, p 285-289, in English.

[21] I.-J. Kim, H. Nanjo, T. Iijima, and T. Abe, Crystallization process of TiNi thin films sputtered at elevated temperatures on Pt/Si oxide/Si and Si oxide/Si substrates, Jpn. J. Appl. Phys., 39, 2000, p 568-571, in English.

[22] R.M.S. Martins, N. Schell, R.J.C. Silva, L. Pereira, K.K. Mahesh, and F.M.B. Fernandes, In-situ study of Ni–Ti thin film growth on a TiN intermediate layer by X-ray diffraction, Sens. Actuators B, 126, 2007, p 332-337, in English.

[23] J.-M. Zhang, F. Ma, and K.-W. Xu, Calculation of the surface energy of bcc metals by using the modified embedded-atom method, Surf. Interface Anal., 35, 2003, p 662-666, in English.

[24] N. Schell, W. Matz, J. Bøttiger, J. Chevallier, and P. Kringhøj, Development of texture in TiN films by use of in situ synchrotron x-ray scattering, J. Appl. Phys., 91, 2002, p 2037-2044, in English.

Substrate	Buffer layer	Deposition TiN		Deposition Ni-Ti	
		Time (min.)	Thickness (nm)	Time (min.)	Thickness (nm)
Si(100)	–	–	–	143	860
SiO_2^*/Si(100)	TiN	3	15	120	720
SiO_2^*/Si(100)	TiN	15	80	120	720
SiO_2^*/Si(100)	TiN	40	215	120	720

* *140 nm amorphous SiO_2 capping layer*

Tab. 1 – Selected deposition parameters for the various samples investigated.

FIGURE CAPTIONS

FIGURE 1: Deposition chamber inserted into the six-circle diffractometer of ROBL: (1) magnetrons, (2) semicircular windows for diffracted beams in horizontal and vertical planes, (3) drive for height adjustment, (4) Eulerian cradle, and (5) detector arm.

FIGURE 2: *In-situ* XRD results for Ni-Ti films deposited directly on a naturally oxidized Si(100) substrate and on TiN buffer layers with thickness values of approximately 15 and 215 nm. Net areas of the diffraction peaks of the B2 phase of Ni-Ti recorded as a function of time.

FIGURE 3: Typical XRR spectra for a 3 min deposition of a TiN buffer layer together with the fitting curve (red line), obtained immediately after TiN growth and before the deposition of the Ni-Ti film on top.

FIGURE 4: XRD spectra with change of temperature obtained at ROBL for the Ni-Ti samples with TiN buffer layers; top - at 470°C, bottom - at RT. The inset (top) shows the results recorded around the B2(211) peak at 100°C (austenitic state) acquired at a laboratory source.

FIGURE 5: Dependence of ER with temperature for the Ni-Ti samples with TiN buffers layers of thickness values of roughly 15, 80 and 215 nm during cooling (top) and heating (bottom). The dot line is used to emphasis the variation of the resistivity during the R-phase transformation (including distortion) on cooling for the different samples.

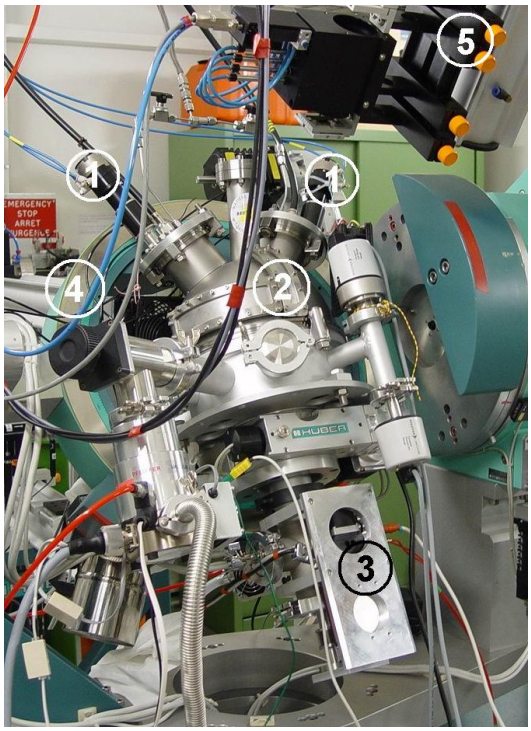

Figure 1

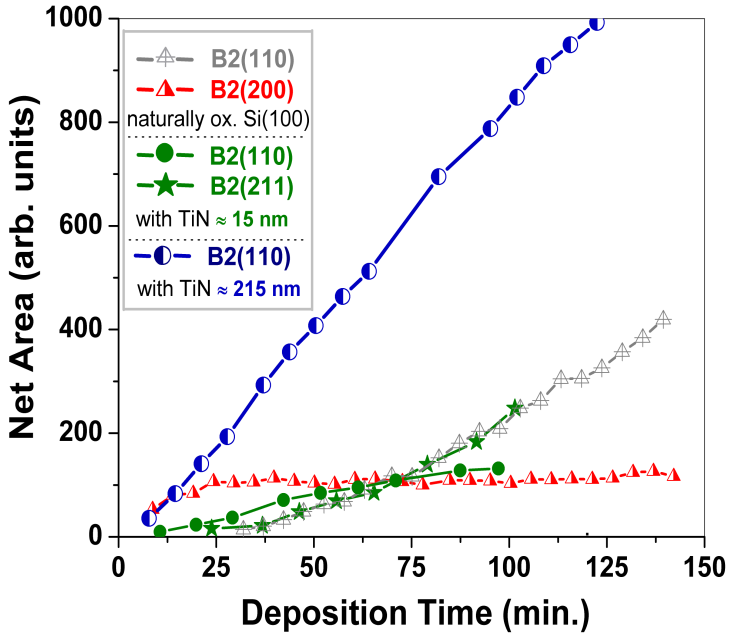
B2(110)
B2(200)
naturally ox. Si(100)
B2(110)
B2(211)
with TiN ≈ 15 nm
B2(110)
with TiN ≈ 215 nm
Net Area (arb. units)
Deposition Time (min.)
0
200
400
600
800
1000
0
25
50
75
100
125
150

Figure 2

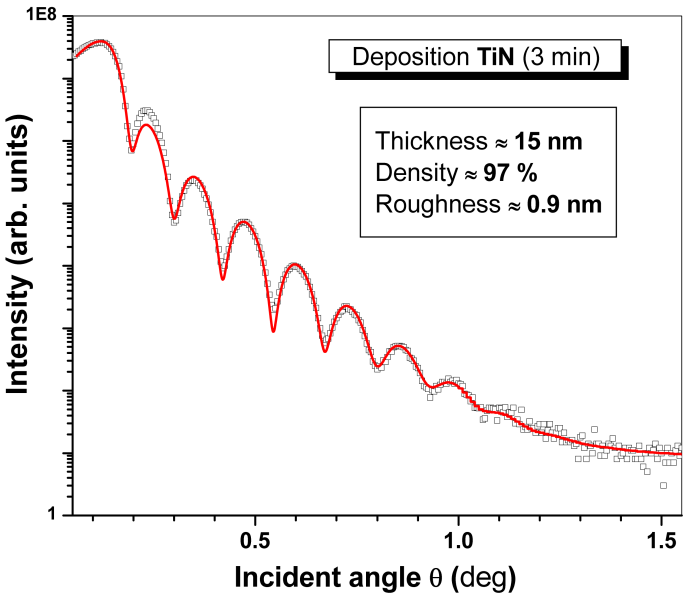
1E8
1
Intensity (arb. units)
0.5
1.0
1.5
Incident angle θ (deg)
Deposition TiN (3 min)
Thickness ≈ 15 nm
Density ≈ 97 %
Roughness ≈ 0.9 nm

Figure 3

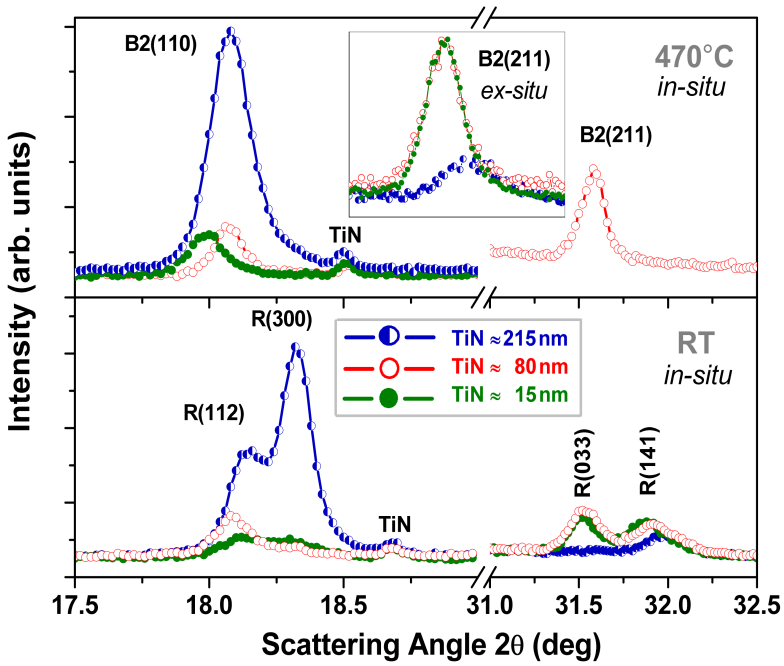
B2(110)
B2(211)
ex-situ
470°C
in-situ
B2(211)
TiN
R(300)
TiN ≈215nm
TiN ≈ 80nm
TiN ≈ 15nm
RT
in-situ
R(112)
R(033)
R(141)
TiN
17.5
18.0
18.5
31.0
31.5
32.0
32.5
Intensity (arb. units)
Scattering Angle 2θ (deg)

Figure 4

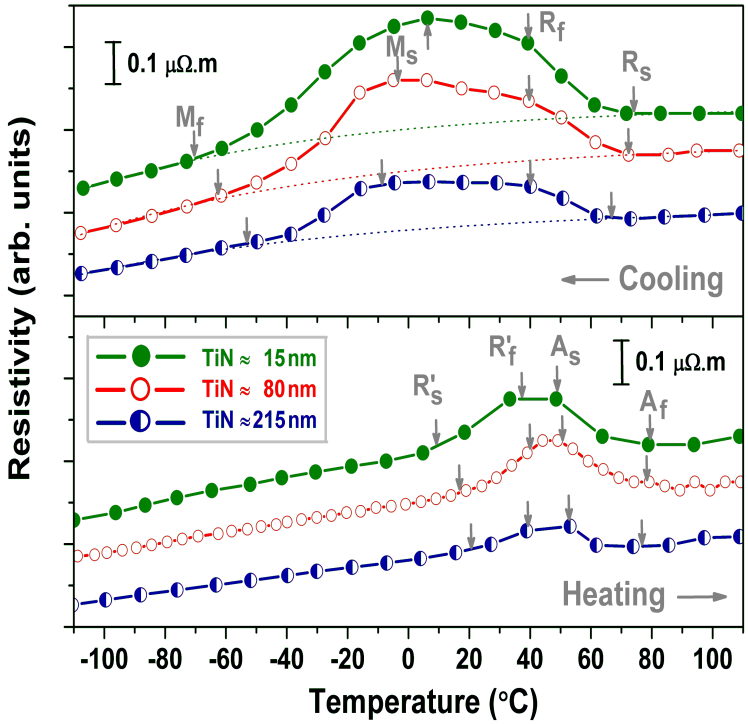
Resistivity (arb. units)
0.1 μΩ.m
Ms
Rf
Rs
Mf
Cooling
TiN ≈ 15nm
TiN ≈ 80nm
TiN ≈215nm
R'f
As
0.1 μΩ.m
R's
Af
Heating
-100 -80 -60 -40 -20 0 20 40 60 80 100
Temperature (°C)

Figure 5